



Inversion algorithm for non-spherical dust particle size distributions

Siyu Cai¹ · Jiandong Mao¹ · Hu Zhao¹ · Chunyan Zhou¹ · Xin Gong¹ · Hongjiang Sheng¹

Received: 25 September 2018 / Accepted: 18 March 2019 / Published online: 1 April 2019
© The Optical Society of Japan 2019

Abstract

Dust particles are the main aerosol component of the atmosphere, and can influence human, environmental, and ecological health. Particle size distribution is an important aerosol micro-physical parameter that denotes the concentration distribution of particles of different radii and can determine the extinction characteristics of these particles. In traditional inversion algorithms, the aerosol is generally assumed to be spherical according to Mie theory, and the relationship between aerosol optical thickness and particle size distribution is described by the Fredholm integral equation of the first kind. For non-spherical dust particles, this spherical assumption is obviously unreasonable and yields unreliable results. Therefore, we developed an algorithm assuming non-spherical particles for inversion of dust particle size distributions. In the case of non-spherical particles, the extinction efficiency factor kernel functions of the ellipsoid were calculated using the anomalous diffraction approximation method, and the kernel function of Mie scattering theory was substituted with these new kernel functions. Moreover, the Phillips–Twomey method was employed to solve the Fredholm integral equation of the first kind using aerosol optical thickness data from a CE-318 sun photometer. To verify the feasibility of the anomalous diffraction approximation method, experiments were carried out under sunny, dusty, windy and hazy weather conditions. These experiments showed that the extinction kernel function for non-spherical particles obtained using the anomalous diffraction approximation method is suitable for inversion of non-spherical dust particle size distributions under different weather conditions in the Yinchuan area.

Keywords Dust aerosol · Non-spherical particle · Anomalous diffraction approximation · Particle size distribution

1 Introduction

Aerosols are ubiquitous components of the atmosphere with no constant chemical composition. These aerosol particles influence energy exchange within the Earth's atmosphere by absorbing and scattering solar radiation, which in turn affects its climate. In recent years, concurrent with the rapid development of China's economy and acceleration of its urbanization, the quality of the atmospheric environment has obviously deteriorated, which has affected quality of life in urban environments. Research on the properties and characteristics of atmospheric aerosols has great practical significance to this pollution issue, making it a focus of atmospheric science [1].

Dust aerosol is an important part of the atmospheric aerosol. It has a crucial impact on human activities and the atmospheric environment, making it imperative to carry out research on dust aerosol [2]. Regarding global warming, the Earth appears to have an extremely complex feedback mechanism and dust storms may be the “refrigerant” of global warming. Dust particles have important effects on the Earth's environment via three main processes: (1) blocking solar radiation from entering the Earth's surface, known as the “parasol effect” [3]; (2) affecting the formation of cloud, radiation characteristics and precipitation by acting as cloud condensation nuclei, resulting in indirect climate effects, known as the “ice nucleation effect” [4]; and (3) increasing iron in the ocean through settling of transported dust, which can increase plankton populations and enhance the amounts of carbon dioxide consumed, leading to a decrease in global temperatures; this is known as the “iron fertilizer effect” [5].

Sun photometers and multi-wavelength lidar, as indispensable tools and methods for atmospheric remote sensing, can facilitate effective real-time monitoring of aerosol parameters, such as aerosol optical thickness (AOT), extinction coefficients and particle size distributions.

✉ Jiandong Mao
mao_jiandong@163.com

¹ School of Electrical and Information Engineering, North Minu University, No. 204, North Wenchang Road, Yinchuan 750021, China

To study the characteristics of atmospheric aerosols in different regions of the world in detail, large-scale and multi-band sun photometer observation networks have been established, such as the AEROSOL ROBOTIC NETWORK (AERONET) [6], SKYradiometer NETWORK (SKYNET) [7, 8], Global Atmosphere Watch Precision Filter Radiometer (GAW PFR) network [9] and the China Aerosol Research Network (CARSONET) [10]. In these networks, sun photometers are the main instruments of observation. They not only automatically track the sun, making direct radiation measurements, but also measure sky radiance along the solar principle plane and along the solar almucantar. Because they obtain real-time and long-term observations, they play an important role in atmospheric environmental and dust storm monitoring, in studies of aerosol–climate effects, as well as in verification of satellite remote sensing products.

When determining aerosol optical and micro-physical properties, the inversion of non-spherical particle size distributions is a frontier issue that needs to be studied in detail [11]. Currently, when using traditional particle size distribution inversion algorithms based on classical Mie scattering theory to calculate extinction efficiency factor kernel function [12], we need to assume that the particle is spherical. For a regular spherical aerosol particle, the inversion error based on this assumption is small, but for non-spherical dust aerosols, there is large error involved in inversion of the particle size distribution.

For SKYNET, Olmo et al. (2005) substituted the kernel based on Mie scattering theory in the SKYRAD.PACK algorithm by one derived for spheroidal particles, and retrieved aerosol optical properties using direct and sky-radiance measurements of a sun photometer [13]. In 2010, Kobayashi et al. also used ellipsoid particle approximation in the SKYRAD.PACK algorithm, which markedly improved the algorithm [14]. To improve aerosol inversion of AERONET observation network data, Dubovik and King (2000) established the Dubovik algorithm using sky radiation measurement data. This algorithm uses an ellipsoid to represent non-spherical particles and distinguishes between fine- and coarse-mode particles. It can be used to retrieve the columnar particle size distribution, refractive index, single scattering albedo, volume backscattering and extinction coefficient [15]. Although both the Dubovik and the improved SKYRAD.PACK algorithm incorporate ellipsoidal particles and provide some research results, the specifications of these algorithms are not publicly available and cannot be used directly.

In recent years, some researchers have carried out limited theoretical studies of the light scattering properties of non-spherical particles, and proposed several calculation methods to determine the non-spherical particle extinction efficiency factor, including the anomalous diffraction approximation (ADA) method, Rayleigh approximation method, T matrix method, finite difference time domain method, and discrete

dipole approximation method. As one of the most effective methods, the ADA method based on Fresnel diffraction theory can be used to calculate the extinction kernel function of ellipsoidal and cylindrical particles in random orientations. Van de Hulst (1981) originally introduced the ADA method (also known as the van de Hulst approximation) to calculate light scattering by particles, which is valid for optically soft particles. In this case, the extinction and absorption efficiencies of randomly oriented particles can be determined using the ratio of particle volume to the projected area [16]. Franssens (2001) presented a new analytical inversion formula that allows the direct computation of the size distribution as an integral over the spectral extinction function, as well as an indirect inversion algorithm that can be used for scarce and noisy extinction measurements [17]. Sun and Fu (2001) compared a simplified

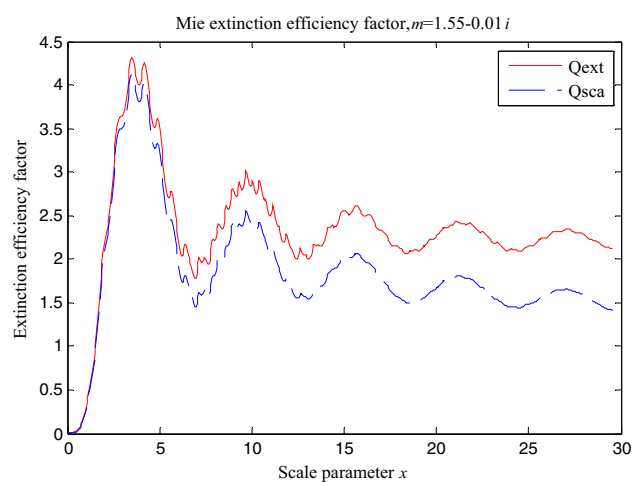


Fig. 1 Relationship between extinction and scattering efficiency factor and the scale parameter. m is the complex refractive index

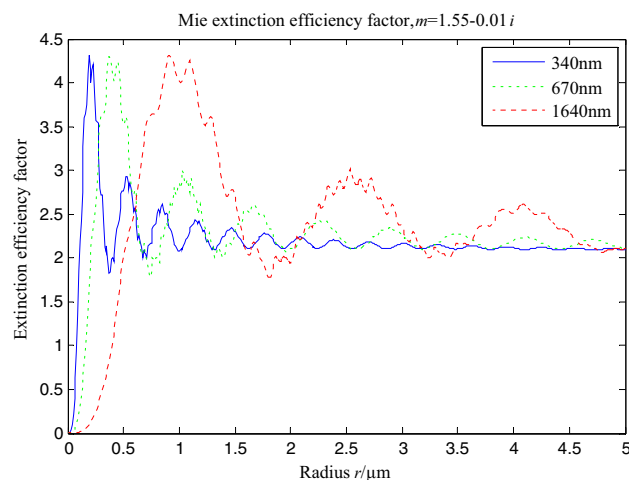


Fig. 2 The extinction efficiency factors derived from Mie scattering theory for spherical particles at 340, 670 and 1640 nm wavelengths

ADA with the original ADA for randomly oriented particles with different shapes and found some significant differences in extinction and absorption efficiencies [18]. Xu and Lax (2003) showed that ADA of extinction of light by soft particles was determined by a statistical distribution of the geometrical paths of individual rays inside the particles; they derived analytical formulas for this extinction using a Gaussian distribution of the geometrical paths of the rays [19]. Tang and coworkers investigated the feasibility and limitations of using the ADA to calculate the extinction efficiency of non-spherical particles; they used ADA instead of Mie extinction efficiency to retrieve the particle size distributions based on a genetic algorithm [20, 21]. Paramonov (2012) proved there is an optical equivalence of randomly oriented ellipsoidal particles and polydisperse spheroidal and spherical particles using the analytical potential of Rayleigh–Gans–Debye theory and ADA; these results were used to develop an optical classification of isotropic ensembles of ellipsoidal particles [22].

In the context of scattering theory, the extinction kernel function of the spherical particles from Mie scattering theory can be substituted by the new kernel function for non-spherical particles derived from the ADA method. Moreover, the functional relationship between the extinction efficiency factor and particle size distribution remains the Fredholm integral equation of the first kind, for which the Phillips–Twomey (P–T) method is the most appropriate solution method [22, 23]. Undoubtedly, using both ADA and P–T methods, it is feasible to retrieve non-spherical dust particle size distributions using AOT data from a sun photometer or multi-wavelength lidar.

2 Light scattering theory

2.1 Mie scattering theory

At the beginning of the twentieth century, to solve the scattering problem of uniform spherical particles, the German scientist Mie established a scattering theory based on electromagnetic theory, which is also known as coarse-particle scattering theory. Mie scattering theory provides an exact solution to the scattering of planar waves by uniform spherical particles in an electromagnetic field, derived from Maxwell's equations. In addition, Mie scattering theory defines scattering laws for uniform spherical particles of arbitrary diameter and arbitrary composition.

According to classical Mie scattering theory [16], we can determine the scattering particle's scale parameter, the radius of particle; the complex refractive index of the scattering particle, and both real and the imaginary parts of complex refractive index.

In this paper, the complex refractive index m is assumed to be $1.55-0.01i$ [24, 25], and the scale parameter range

is assumed to be 0–25. Figure 1 shows the relationship between the extinction and scattering efficiency factor and the scale parameter $x = 2\pi r/\lambda$, where r is the particle radius

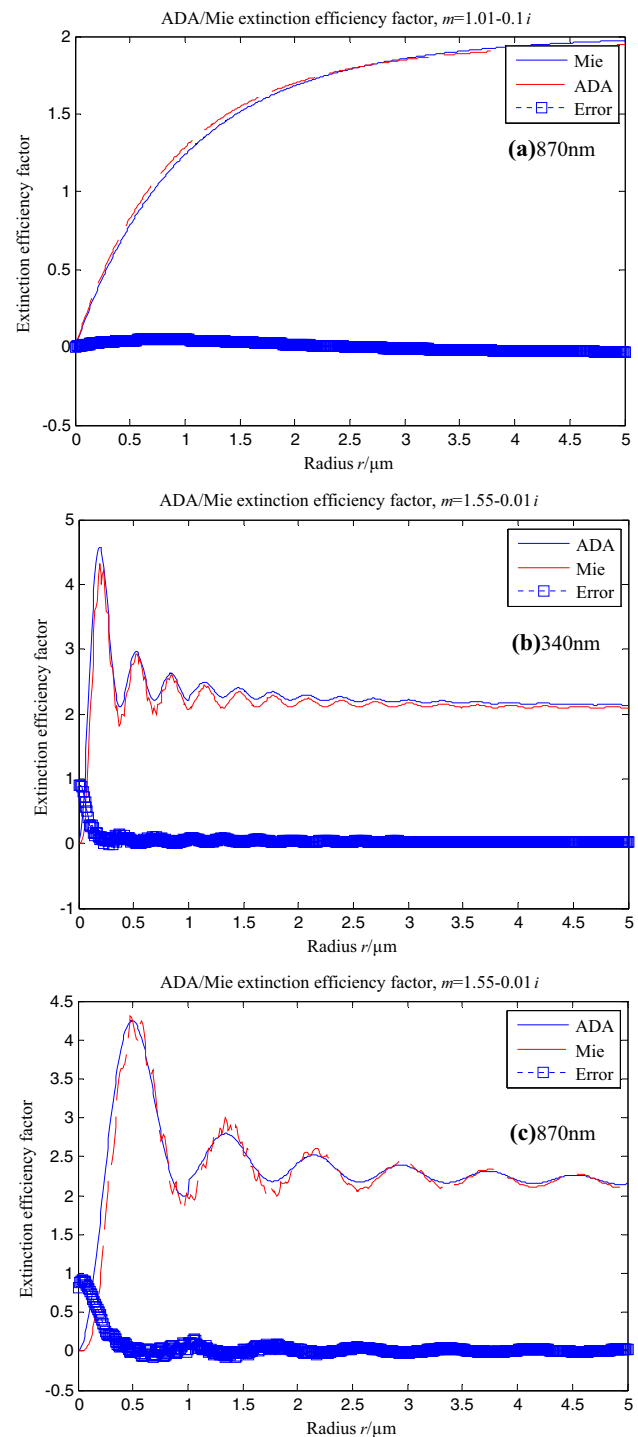


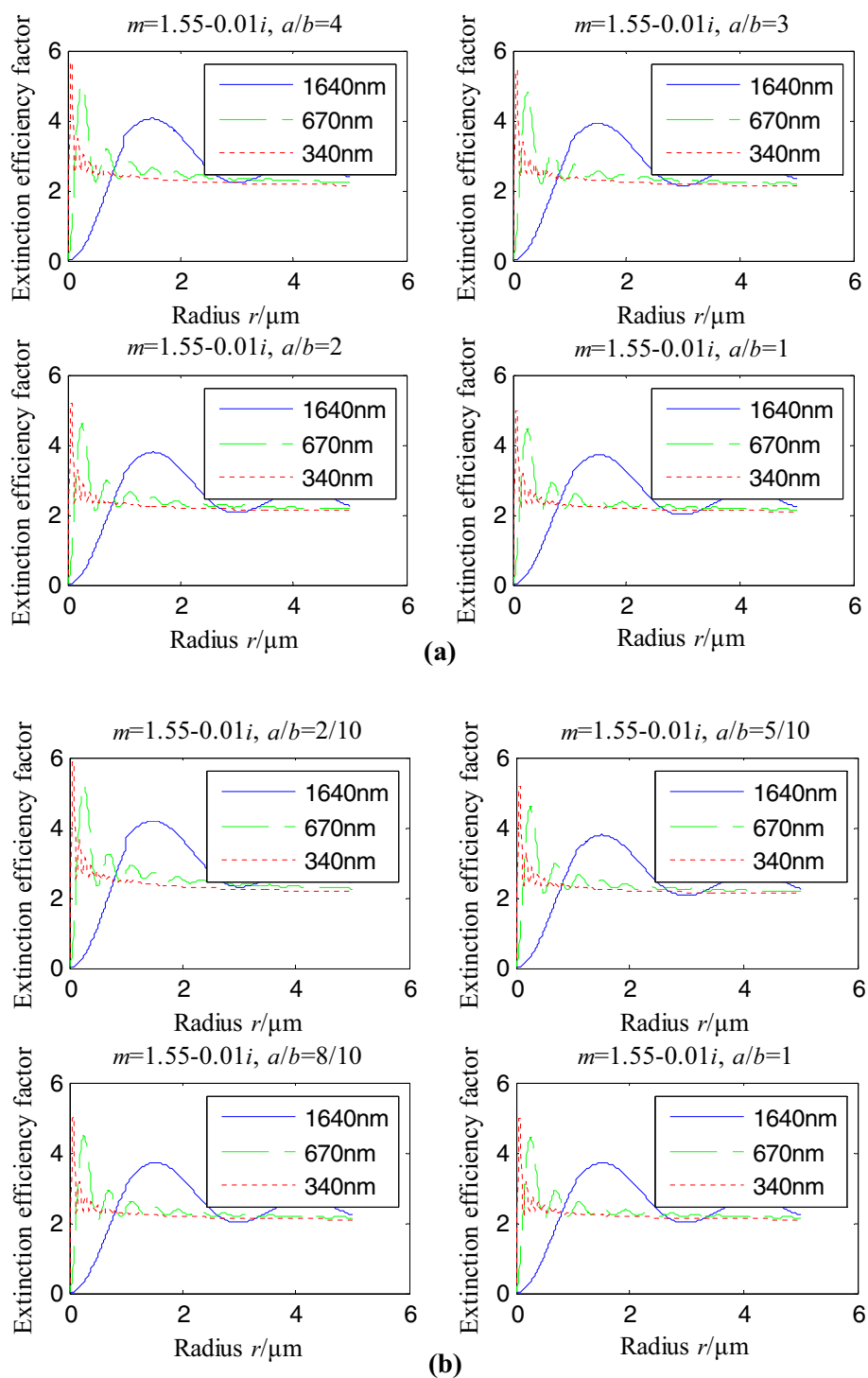
Fig. 3 Comparison of the extinction efficiency factors and relative errors for spherical particles using the Mie scattering theory and the ADA method for (a) an incident light wavelength of 870 nm and complex refractive index of $1.01-0.1i$, (b) 340 nm and $1.55-0.01i$, and (c) 870 nm and $1.55-0.01i$

and λ is the wavelength of incident light. Clearly, the extinction efficiency factor is positively correlated with the scattering efficiency factor [16]. Moreover, it should be pointed out that because complex refractive index is a function of wavelength, the wavelength affects complex refractive index to a large extent. The real part of the refractive index has little change in the visible wavelength, but the imaginary part of the refractive index varies greatly in the visible and infrared

wavelengths, even with an order of magnitude difference, which is mainly related to the existence of absorption bands in these wavelengths.

Figure 2 shows the extinction efficiency factors of spherical particles at 340, 670 and 1640 nm wavelengths, based on Mie scattering theory. In Fig. 2, the maxima of the extinction efficiency factors of these three wavelengths are concentrated within the particle size range of 0.2–1.0 μm . As

Fig. 4 The radius dependence of the extinction efficiency factors for each wavelength derived from ADA for (a) long ellipsoidal particles, and (b) flat ellipsoidal particles with different aspect ratios



the wavelength increases, the maximum peak moves in the direction of increasing particle size (radius). The extinction efficiency factors show oscillation in their convergence process, which gradually tends to a value of two; the smaller the wavelength, the faster the convergence, and the weaker the oscillation [16].

2.2 ADA theory

2.2.1 Comparison of spherical particle extinction efficiency factors

According to ADA theory [12–18] for spherical particles, the extinction efficiency factor is given by [16–23, 26]:

$$Q_{ad} = 4 \operatorname{Re} \left[\frac{1}{2} - i \frac{\exp(-iw)}{w} + \frac{1 - \exp(-iw)}{w^2} \right], \quad (1)$$

where $w = kD(m - 1)/\lambda$, λ is the wavelength of incident light; D is the diameter of the spherical particles; and k is the wave number in a vacuum.

To establish any inversion effect of using the ADA method, the extinction efficiency factors were calculated using Mie scattering theory and the ADA method, respectively. Figure 3 shows the comparison of extinction efficiency factors and relative errors for spherical particles, based on these two methods. In Fig. 3 (1), the complex refractive index is $1.01 - 0.1i$ and the incident light wavelength is 870 nm. It is obvious that for spherical particles the inversion results of these two methods are in good agreement for effective particle radii of $0.01 - 5 \mu\text{m}$. Therefore, the extinction kernel function derived from the ADA method can be used to replace the corresponding kernel function from Mie theory, providing a reliable basis to carry out this process with non-spherical particles.

In Fig. 3b, c, the relative complex refractive indices are all $1.55 - 0.01i$, while the incident light wavelengths are 870 and 340 nm, respectively. The oscillating convergence of extinction efficiency factors retrieved using the ADA method and Mie scattering theory are basically the same, although their relative error curves fluctuate slightly. The difference between the two methods for radii from 0 to $0.5 \mu\text{m}$ is obvious, after which this difference gradually approaches zero. Although the error fluctuates with increasing wavelength, these fluctuations are within a reasonable range, suggesting that the new extinction kernel function calculated from the ADA method can effectively replace the extinction kernel function from Mie scattering theory.

2.2.2 Extinction efficiency factor of ellipsoidal particles using the ADA method

When the angle θ between the rotation axis of the ellipsoidal particle and the direction of incident light is arbitrary, the

extinction efficiency factor of an ellipsoidal particle can be retrieved using the ADA method [16–23, 26], as follows:

$$Q_{ade} = 4 \operatorname{Re} \left[\frac{1}{2} - i \frac{\exp(-iv)}{v} + \frac{1 - \exp(-iv)}{v^2} \right], \quad (2)$$

where $v = 2ka(m - 1)/\lambda g$; $g = \sqrt{\cos^2(\theta) + r^2 \sin^2(\theta)}$; and a is the half shaft length of the ellipsoidal particle’s rotation axis. The ellipsoidal particle boundary term is given by

$$Q_{edge} = \frac{4c_0 r^{2/3}}{\pi(kb)^{2/3} g^2} \int_0^{\pi/2} q^{4/3} d\chi, \quad (3)$$

where $g = \sqrt{\cos^2(\theta) + r^2 \sin^2(\theta)}$; $q = (\sin^2 \chi + g^2 \cos^2 \chi)^{1/2}$; θ is the angle between the incident light direction and the rotation axis of the ellipsoidal particle; χ is the parametric angle of the penumbral ellipse; b is the length of the semi

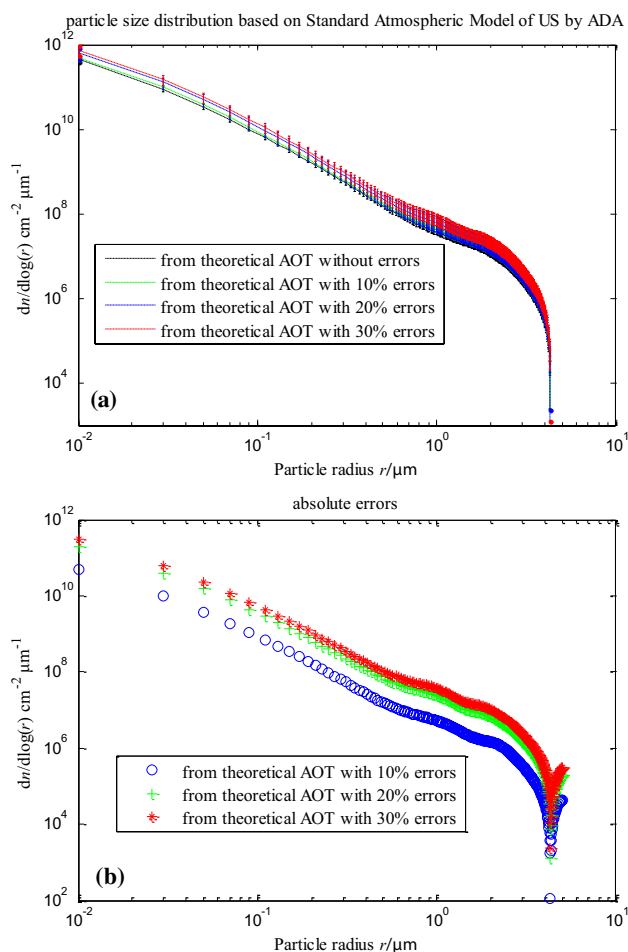


Fig. 5 **a** Particle size distributions and error bars retrieved from theoretical aerosol optical thickness (AOT) data and AOTs with 10%, 20% and 30% random errors, respectively. **(b)** Absolute errors reflecting the difference between the theoretical particle size distribution and those retrieved from AOTs with added 10%, 20% and 30% random errors, respectively

Table 1 The center wavelength and bandwidths of the CE-318 sun photometer

| | | | | | | | | |
|------------------------|-----|-----|-----|-----|-----|-----|------|------|
| Central wavelength, nm | 340 | 380 | 440 | 500 | 670 | 870 | 1020 | 1640 |
| Bandwidth, nm | 2 | 2 | 10 | 10 | 10 | 10 | 10 | 60 |

axis of the ellipsoidal particle; $s = a/b$ is the aspect ratio, i.e., for a long ellipsoid, $s > 1$, and for a flat ellipsoid, $s < 1$; and c_0 is a constant equal to 0.99613.

Thus, the average extinction efficiency factor \bar{Q}_{ext} of an ellipsoidal particle in any direction is given by [16–23, 26]:

$$\bar{Q}_{ad} = \frac{\int_0^{\pi/2} Q_{ad} \sin^2(\theta) d\theta}{\int_0^{\pi/2} \sin^2(\theta) d\theta}, \tag{4}$$

$$\bar{Q}_{edge} = \frac{\int_0^{\pi/2} Q_{edge} S_2 \sin(\theta) d\theta}{\int_0^{\pi/2} S_2 \sin(\theta) d\theta}, \tag{5}$$

where S_2 is the projected area of ellipsoidal particles in the direction perpendicular to the incident light.

$$\bar{Q}_{ext} = \bar{Q}_{ad} + \bar{Q}_{edge}. \tag{6}$$

Figure 4 shows the radius dependence of the extinction efficiency factors for each wavelength derived from ADA for long and flat ellipsoidal particles having different aspect ratios. In Fig. 4, the complex refractive index is $1.55 - 0.01i$, the incident light wavelengths are 1640, 670 and 340 nm, while the angles between the incident light and ellipsoidal particle rotation axes are all 90° . When the ellipsoidal particles maintain a fixed aspect ratio and the incident light has different wavelengths, the extinction efficiency factors from the ADA method have similar characteristics to these derived from Mie scattering theory. In both cases, increases in the length of the half shaft cause the extinction efficiency factors to oscillate faster, while the amplitude rapidly converges to a value of two and becomes stable.

3 Inversion of particle size distributions using the Phillips–Twomey method

King et al. (1978) proposed that the atmospheric AOTs obtained by measuring the direct solar radiation intensity of the whole atmosphere can be used to retrieve particle size distributions [27]. Under the assumption of spherical particles, given the small change of the refractive index m of aerosol in visible and near-infrared wavelengths, it can be defined as a constant. Therefore, the relationship between AOTs and particle size distribution can be expressed as [28–33]:

$$\begin{aligned} \tau_i(\lambda) &= \int_0^{Z_M} \int_{r_0}^{r_M} \pi r^2 Q_{ext}(r, \lambda_i, m) N(r, z) dr dz \\ &= \int_{r_0}^{r_M} \pi r^2 Q_{ext}(r, \lambda_i, m) N(r) dr, \end{aligned} \tag{7}$$

where Q_{ext} is the extinction efficiency factor, r is the particle radius, r_0 and r_M are the upper and lower limits of the radii, $N(r, z)$ is the local aerosol spectrum distribution, and $N(r) = \int_0^{Z_M} N(r, z) dz$ is the particle size distribution to be solved. Clearly, this relationship is described by the Fredholm integral equation of the first kind.

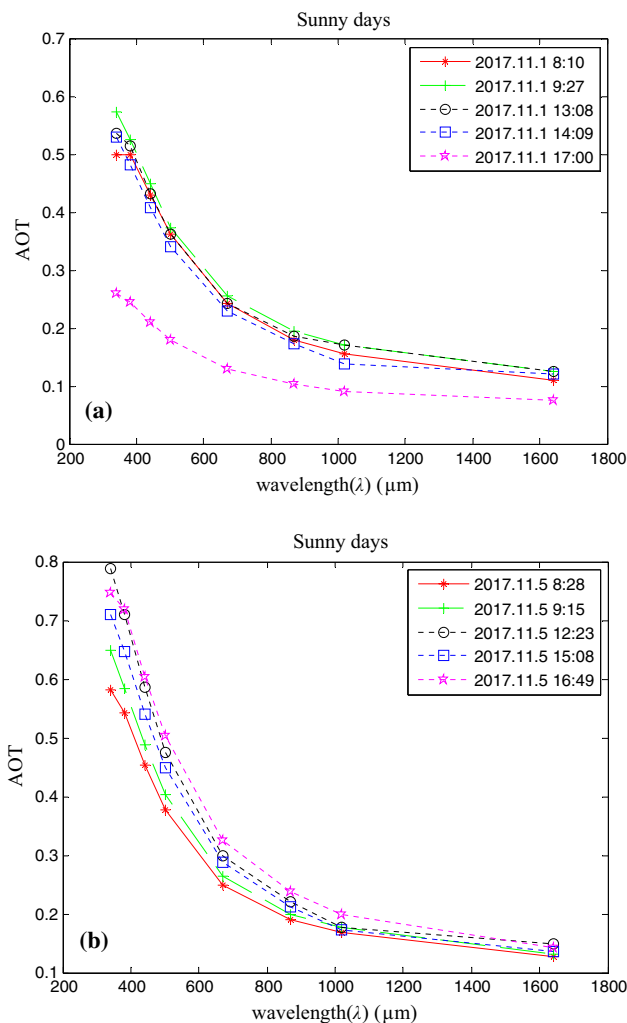


Fig. 6 Diurnal variation in aerosol optical thickness (AOT) under sunny conditions on (a) 1 November 2017; and (b) 5 November 2017 at selected local times (see figure legend)

Generally, continental dust particle size distributions can be described using a Junge distribution:

$$N(r) = Cr^{-(v+a)} \tag{8}$$

Thus, when v is determined, the particle size distribution $N(r)$ can be obtained.

Because actual particle size distributions are not smooth functions, they change greatly with r , leading to instability of the solution. Using the method proposed by Herman et al. (1971) [34], the size distribution $N(r)$ can be decomposed into the product of the fast variable function $h(r)$ and the slow variable function $f(r)$ [34], i.e., $N(r) = h(r)f(r)$. Now, Eq. (7) can be written as

$$g_i = \int_{r_0}^{r_M} K_i(r, m)h(r)f(r)dr, \tag{9}$$

where g_i corresponds to the AOT and $K_i(r, m)$ is the kernel function, corresponding to $\pi r^2 Q_{ext}(r, \lambda_i, m)$. Eq. (9) can be converted to matrix form [27]:

$$\vec{g} = A\vec{f} + \vec{\varepsilon}, \tag{10}$$

where \vec{f} is the vector to be solved, $\vec{\varepsilon}$ is the error vector, \vec{g} is the known vector, and A is the coefficient matrix, having elements defined by

$$A_{ij} = \int_{r_j}^{r_{j+1}} K_i(r, m)h_j(r)dr, \quad i = 1, 2, \dots, N, j = 1, 2, \dots, M. \tag{11}$$

When the P–T method is applied to this constrained linear inversion equation, the smooth constraint of the second derivative is introduced. Therefore, the solution of Eq. (10) is

$$\vec{f} = (A^T A + \gamma H)^{-1} A^T \vec{g}, \tag{12}$$

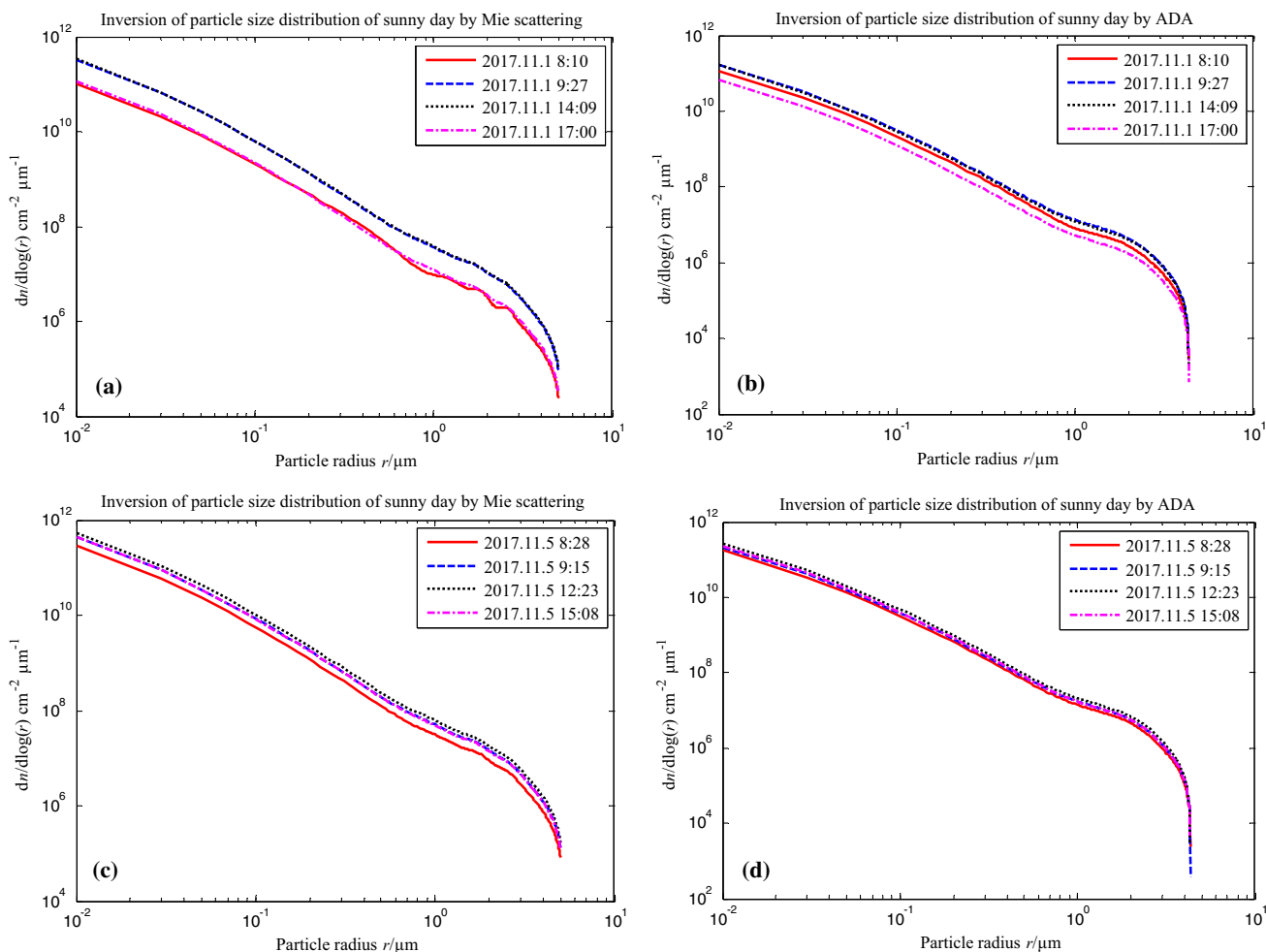


Fig. 7 Diurnal variation in particle size distributions retrieved from aerosol optical thickness (AOT) for the two sunny days shown in Fig. 6 (1 and 5 November 2017), comparing Mie scattering theory and the ADA method

where \vec{f} and \vec{g} are column vectors; A and A^T are the coefficient matrix and its transposed matrix, respectively; γ is the Lagrange smoothing factor; and H is a smoothing matrix [27–33].

To verify the reliability and feasibility of obtaining extinction efficiency factors from the ADA method, some simulations were carried out using theoretical AOTs obtained from the Standard Atmospheric Model of the US (1976). In these simulations, the particle size distribution was inverted using both ADA and P–T methods for long ellipsoidal particles with aspect ratios of two and a complex refractive index of $1.55-0.01i$. To estimate the adaptive capacity of these methods to error, 10%, 20% and 30% random errors were superimposed on the theoretical AOTs. Figure 5a shows the particle size distributions and error bars retrieved from

theoretical AOTs with 10%, 20% and 30% random errors. Figure 5b shows the absolute errors between theoretical particle size distributions and those retrieved from AOTs with 10%, 20% and 30% errors, respectively. It is clear that with increasing error components, the relative errors and absolute error also increased. In the cases of 10% and 20% random errors, the absolute error was minimal, but at a 30% error level, the absolute error was obvious.

It is clear that with the increase of particle radii the retrieval absolute errors gradually decrease, and especially for the small particles with radii smaller than $0.1 \mu\text{m}$, the particle size distribution has very large absolute errors. Moreover, from Figs. 1, 2, 3 and 4, for the extinction and scattering efficiency factor, the smaller the radii is, the more serious the oscillation is. Therefore, in this paper, when the particle size range is larger than $0.1 \mu\text{m}$, the

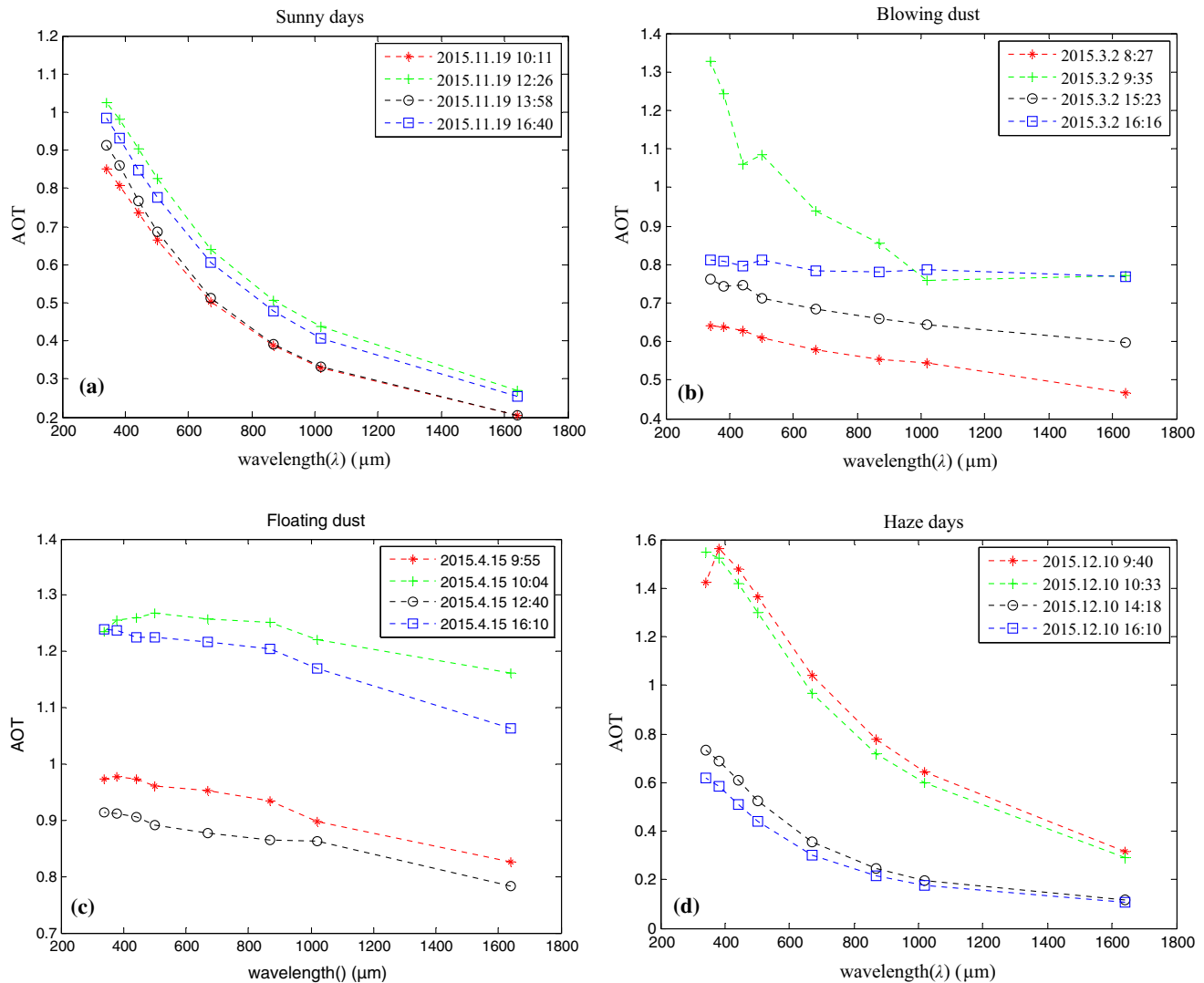


Fig. 8 Diurnal variation in aerosol optical thickness (AOT) values shown on selected dates for selected local times (see figure legends) under (a) sunny; (b) windy (with blowing dust); (c) dusty (with floating dust); and (d) hazy weather conditions

retrieval results are relative reliable. In fact, the optical observation is not sensitive for those particles with radii smaller than 0.1 μm.

4 Analysis of experiment results

Some experiments were performed under dusty, hazy and sunny weather conditions in the Yinchuan area. This area is in northwestern China. It has a mid-temperate semiarid continental climate, with a long winter, warm spring, short hot summer, and cool autumn. It is characterized by large diurnal temperature differences. It often experiences drought. There are four deserts, namely the Badain Jaran, Ulan Buh, Tengger and Mu Us deserts, to the northwest, west, and east of the Yinchuan area. Therefore, the Yinchuan area is the main source of mineral dust particles in northwest China, with dust particles dominating the atmosphere. The AOT data were measured by a CE-318 sun photometer (Cimel Electronique S.A.S, Paris, France), placed on the roof of the five-floor no. 17 teaching building of the North Minzu University in Yinchuan (38°29'49"N, 106°06'12"E). These data were used to retrieve particle size distributions. The CE-318 model makes direct spectral solar radiation measurements within a 1.2° full-field of view every 3 min at wavelength bands of 340, 380, 440, 500, 670, 870, 1020 and 1604 nm. It has automatically detected AOTs for these different bands from sunrise to sunset since September 2012. Table 1 lists the center wavelength and bandwidths of the CE-318 model.

Herein, the Langley plot calibration method was employed to obtain the AOTs. According to the Beer–Lambert–Bouguer law [35]:

$$V(\lambda) = V_0(\lambda)d_s \exp(-M\tau_{\text{atn}}(\lambda))t_g(\lambda), \tag{13}$$

where $V(\lambda)$ is the measured irradiance (in arbitrary units) at wavelength λ , $V_0(\lambda)$ is the calibration coefficient, d_s is the correction factor for the Sun–Earth distance, M is the optical air masses, $\tau(\lambda)_{\text{atn}}$ is the Rayleigh scattering optical thickness of atmospheric molecules and AOT, excluding the effect of absorption gases, while $t_g(\lambda)$ is the transmittance of the absorption gas.

Taking the logarithm of Eq. (13) yields

$$\ln V(\lambda) - \ln d_s - \ln t_g(\lambda) = \ln V_0(\lambda) - m\tau_{\text{atn}}(\lambda). \tag{14}$$

Under very clear atmospheric conditions, some observations were undertaken over a range of air masses (M) during which the optical depth τ remained constant. According to Eq. (14), the values of $\ln V(\lambda) - \ln d_s - \ln t_g(\lambda)$ versus M were plotted as a straight line, having $\ln[V_0(\lambda)]$ as the intercept and $-\tau(\lambda)$ as the slope. In this case, m can be calculated for a given date, time and location (latitude and longitude). In fact, the calibration of CE-318 sun photometer is

performed by an agency of Cimel Company in Beijing with 1-year interval.

Figure 6 shows diurnal changes in AOTs on two sunny winter days during November 2017. The AOTs gradually decreased with increasing wavelength. In Fig. 6a, the diurnal change in AOT was unimodal, with a rise in the early stages of the day and a fall in the later stages of the day, with a peak value at about 09:30 (local time). In Fig. 6b, the AOT values were bimodal, with maxima at 12:00 and 17:00 (local time), respectively. Under sunny conditions, the aerosol particles were assumed to be mainly produced by human activities.

Herein, the particle size distributions were obtained using the P–T method. Figure 7 shows the diurnal variation in the particle size distribution retrieved from AOTs shown in Fig. 6. The particle size distributions were retrieved with different kernel functions, calculated either from Mie scattering theory or from the ADA method, respectively. Under stable sunny conditions, the aerosol particles in the

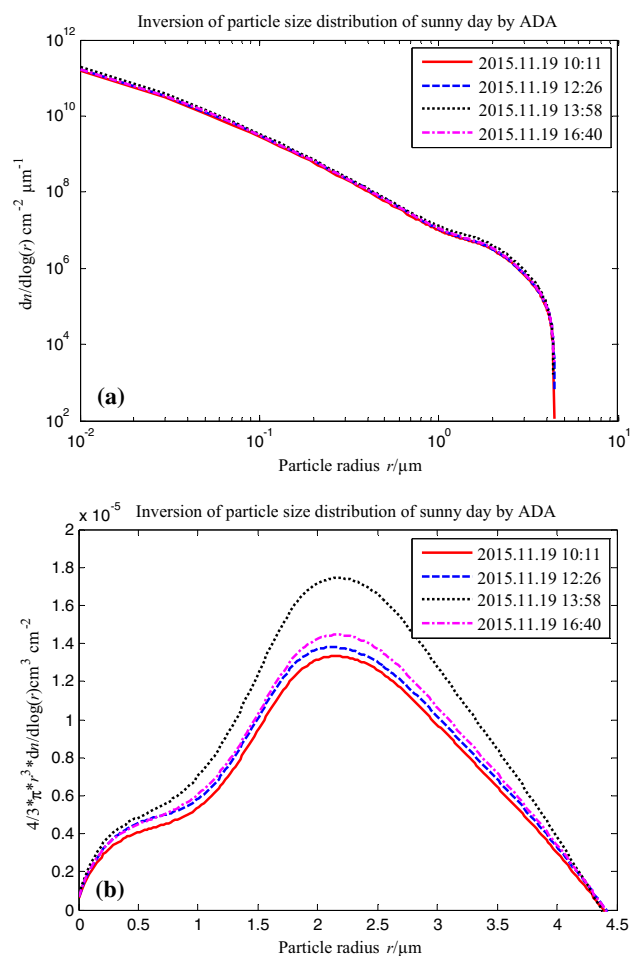


Fig. 9 Diurnal variation in (a) particle number size distributions and (b) volume size distributions shown at selected local times (see legend) over the course of a sunny day (19 November 2015)

atmosphere were relatively stable. In this case, the variation in particle size distributions retrieved using the two methods were also stable and the distributions derived from different methods showed good agreement. Clearly, the kernel function obtained from the ADA method could replace the kernel function from Mie scattering theory, which is valid only for spherical particles.

Therefore, we used the ADA method to retrieve non-spherical dust particle size distributions, where non-spherical particles were assumed to be ellipsoidal particles. The feasibility of this method was evaluated under variable weather conditions, including sunny, dusty, windy and hazy days. We used results of the sunny day to define background values.

Figure 8 shows the diurnal variation of AOTs under different weather conditions. The change in AOTs on dusty and windy days was similar, suggesting a similar content of dust in the atmosphere. In hazy weather, AOTs were mainly

influenced by the exhaust emissions from motor vehicles and micron-sized particulate matter produced from other smoke emission sources in the morning. However, improvement of weather conditions in the afternoon led to AOT changes that were like those on sunny days.

Figure 9 shows the diurnal variation in the non-spherical particle number size distribution and volume size distributions retrieved from the AOTs shown in Fig. 8a on a sunny day. On sunny days, the composition of particles in atmosphere was relatively stable. It is clear from Fig. 9b that particle volume size distributions was bimodal with peaks located at about $0.5\ \mu\text{m}$ and $2.3\ \mu\text{m}$, respectively. From the morning, with increase of human activities and strengthening of ground-air convection caused by air temperatures, the two peaks value gradually increase, reach to maximum at noon and then start to decrease at afternoon.

Figures 10 and 11 show the diurnal variation in particle size distributions under dusty and windy conditions.

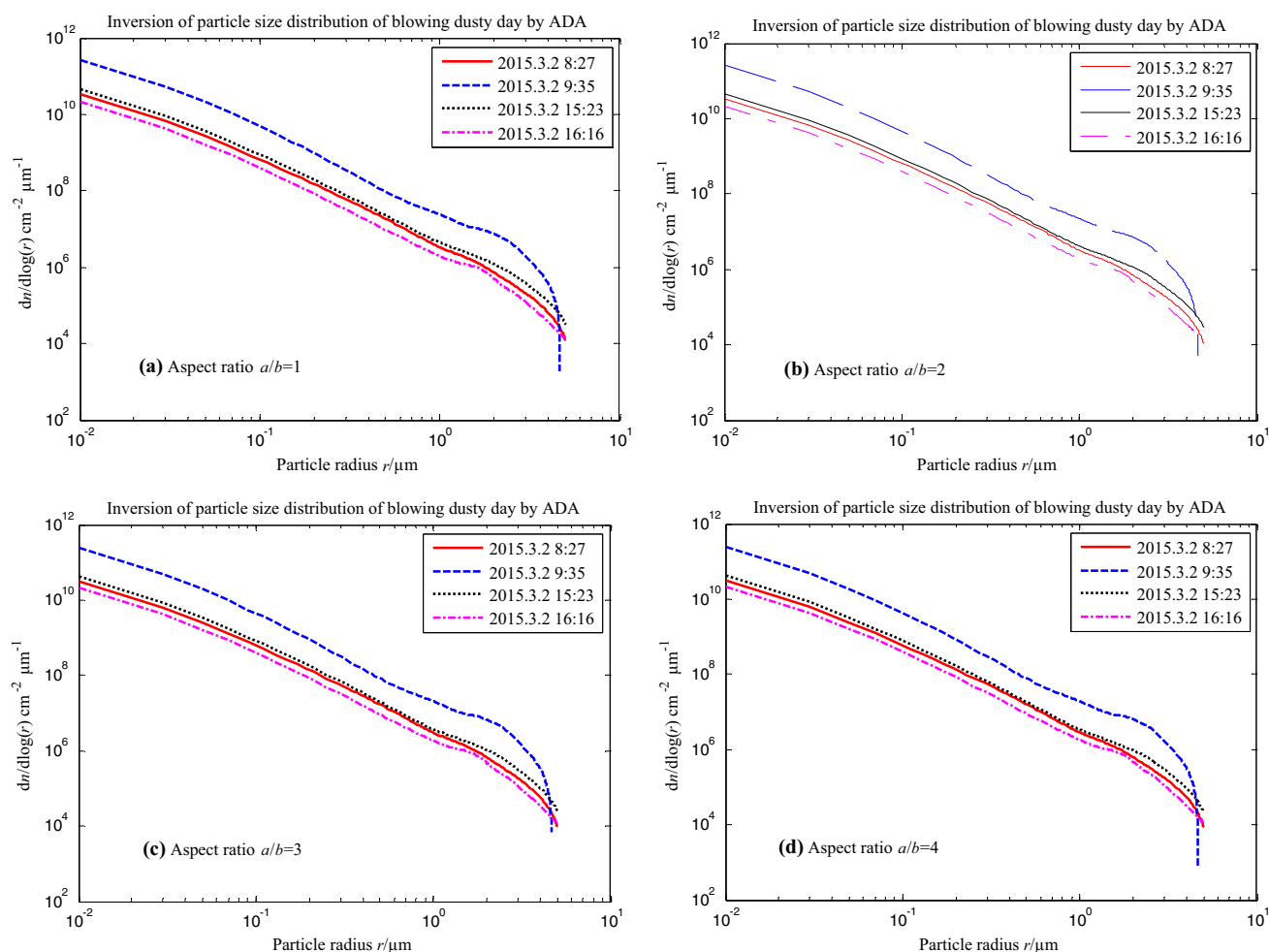


Fig. 10 Diurnal variation of particle size distributions shown at selected local times on a windy day (2 March 2015) using the ADA method for non-spherical particles with different aspect ratios. Aspect ratio is shown in each panel

On dusty days, the dust particles in the atmosphere were dominant. In this case, the particle size distributions were bimodal, with peaks concentrated around 0.8 μm and 2 μm ; these peak locations changed over the course of the day. Under windy conditions, dust particles float in the atmosphere for a long time, accumulating gradually and markedly increasing the particle content of the atmosphere.

Figure 12 shows the diurnal variation in the particle size distribution on a hazy day. On hazy days, the air quality was poor, and the composition of the particles in the atmosphere was complex and variable. Peaks in the particle size distributions were mainly concentrated around 0.6 μm and 1.0 μm . Over time, there was a shift to larger particle sizes, especially by mid-afternoon. Thus, particle concentrations reached the highest levels in the afternoon and gradually decreased as weather conditions improved towards evening.

5 5 Conclusions

The Mie scattering theory can be used to calculate extinction characteristics and retrieve particle size distributions for spherical particles. However, for non-spherical particles, the spherical assumption is obviously unreasonable. Herein, the ADA method was selected to calculate the extinction efficiency factors kernel function of ellipsoidal particles instead. To verify the feasibility of the ADA method, non-spherical dust particle size distributions were retrieved from AOT data measured by a CE-318 sun photometer under different weather conditions in the Yinchuan area. Experimental results show that the ADA method is better suited to inversion of non-spherical dust particle size distributions than traditional methods.

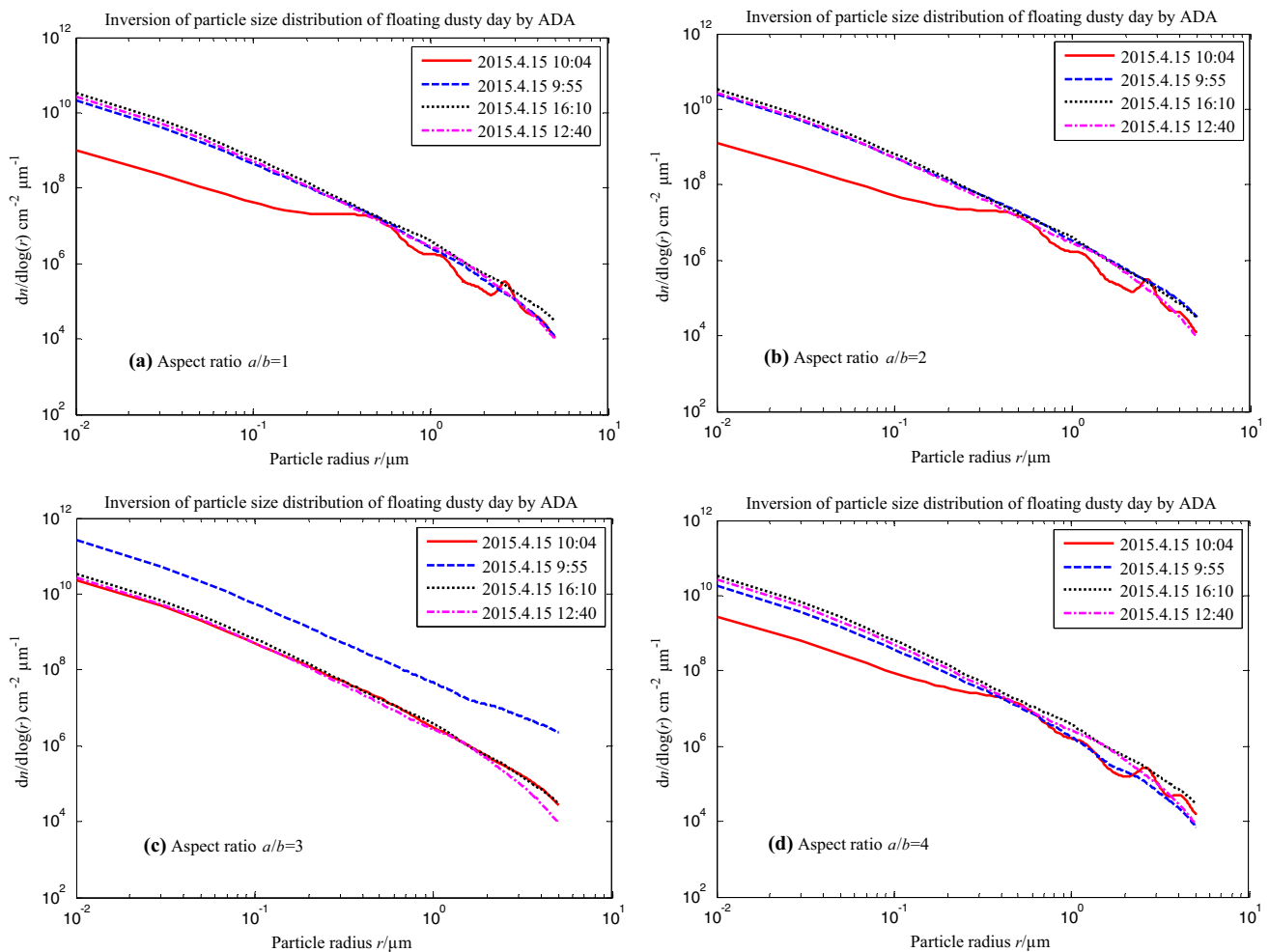


Fig. 11 Diurnal variation of particle size distribution on a dusty day (15 April 2015) using the ADA method for non-spherical particles with different aspect ratios

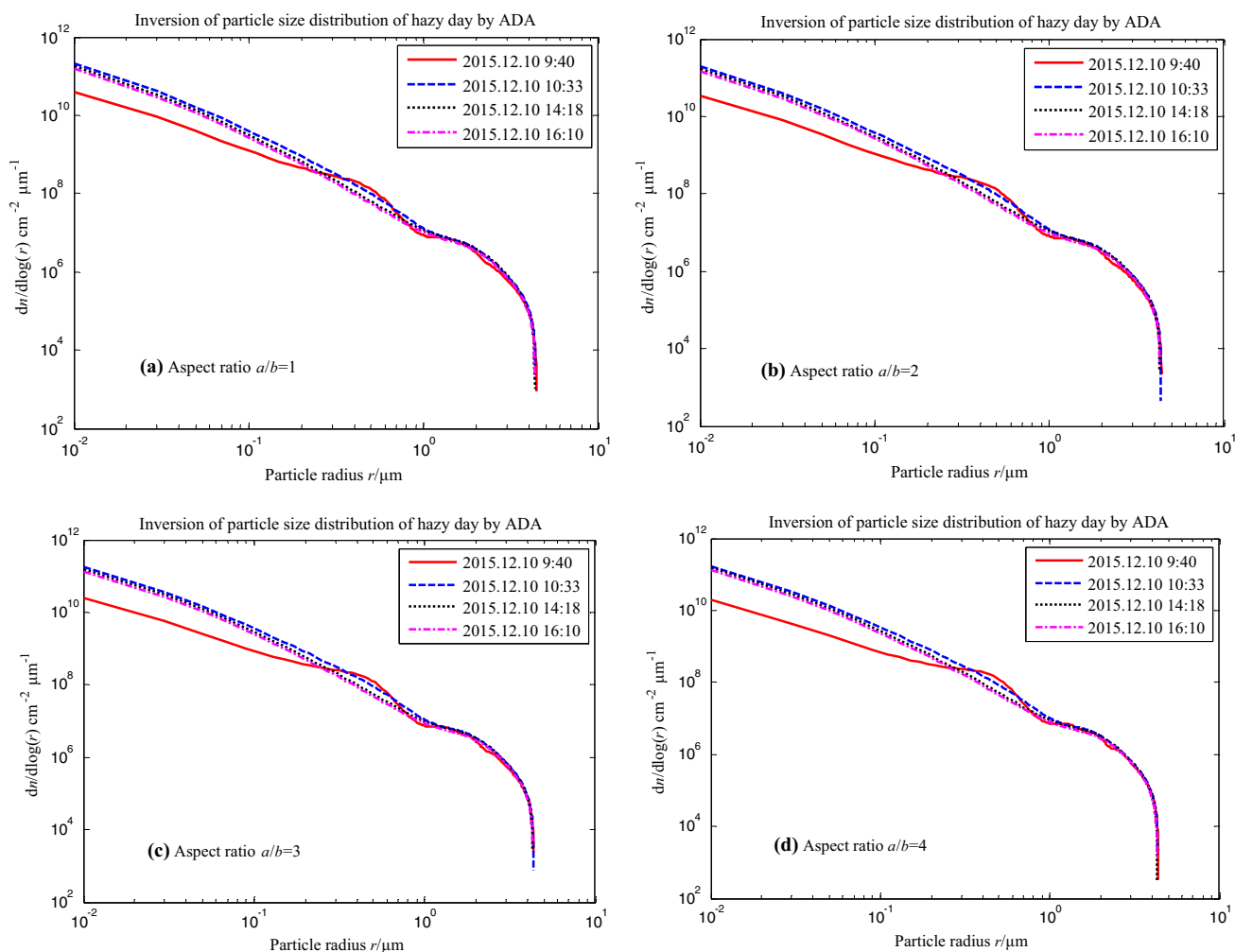


Fig. 12 Diurnal variation of particle size distribution on a hazy day (10 December 2015) using the ADA method for non-spherical particles with different aspect ratios

Acknowledgements This work was supported by the National Natural Science Foundation of China (No. 61765001 and 61565001), Leading Talents of Scientific and Technological Innovation of Ningxia, Plan for Leading Talents of the State Ethnic Affairs Commission of the People's Republic of China, Scientific Research Project of North Minzu University (No. 2016GQR07) and the Innovation Team of Lidar Atmosphere Remote Sensing of Ningxia.

Compliance with ethical standards

Conflict of interest The authors declare that they have no conflicts of interest.

References

- Toledo, F., Garrido, C., Díaz, M., Rondanelli, R., Jorquera, S., Valdivieso, P.: AOT retrieval procedure for distributed measurements with low-cost sun photometers. *J. Geophys. Res.* **123**(2), 1113–1131 (2018)
- Zhang, X., Mao, M.: Orientation-averaged optical properties of nonspherical dust aerosols. *J. Light Scatt.* **29**(1), 16–20 (2017)
- Shi, G.Y., Wang, H., Wang, B.: Sensitivity experiments on the effects of optical properties of dust aerosol on their radiative forcing under clear sky condition. *J. Meteorol. Soc. Jpn* **83**, 333–346 (2005)
- Jia, X., Wang, W., Chen, Y., Huang, J., Chen, J., Zhang, H., Bai, H., Zhang, P.: Influence of dust aerosols on cloud radiative over Northern China. *China Environ. Sci.* **30**(8), 1009–1014 (2010)
- Watson, A.J., Bakker, D.C.E., Ridgwell, A.J., et al.: Effect of iron supply on southern ocean CO₂ uptake and implications for glacial atmospheric CO₂. *Nature* **407**(6805), 730–733 (2005)
- Holben, B.N., Eck, T.F., Slutsker, I., Tanre, D., Buis, J.P., Setzer, A., Vermote, E., Reagan, J.A., Kaufman, Y.J., Nakajima, T., Lavenu, F., Jankowiak, I., Smirnov, A.: AERONET-A federated instrument network and data archive for aerosol characterization. *Rem. Sens. Environ.* **66**(1), 1–16 (1998)
- Kim, D.H., Sohn, B.J., Nakajima, T., Takamura, T., Takemura, T., Choi, B.C., Yoon, S.C.: Aerosol optical properties over east Asia determined from ground-based sky radiation measurements. *J. Geophys. Res.* **109**(2), D02209 (2004)

8. Uchiyama, A., Yamazaki, A., Togawa, H., Asano, J.: Characteristics of aeolian dust observed by sky-radiometer in the Intensive observation period 1 (IOP1). *J. Meteor. Soc. Jpn.* **83A**(3), 91–305 (2005)
9. Wehrli, C., Calibration of filter radiometers for the GAW Aerosol Optical Depth network at Jungfraujoch and Mauna Loa. In: Proceedings of ARJ workshop, SANW congress, Davos, Switzerland, 70–71: (2002)
10. Che, H., Zhang, X., Chen, H., Damiri, B., Goloub, P., Li, Z., Zhang, X., Wei, Y., Zhou, H., Dong, F., Li, D., Zhou, T.: Instrument calibration and aerosol optical depth (AOD) validation of the China aerosol remote sensing network (CARSONET). *J. Geophys. Res.* **114**, (D3) (2009)
11. Song, Y., Lu, L., Li, S., Xin, W., Yan, Q., Hua, D.: Analysis of light scattering properties of non-spherical aerosol particles. *J. Xi'an Univ. Technol.* **33**(2), 233–239 (2017)
12. Zhang, H., Zhao, W., Ren, D., Qu, Y., Song, B.: Improved algorithm of Mie scattering parameter based on matlab. *J. Light Scatt.*, 20 (2), 102–110 (2008)
13. Olmo, F.J., Quirantes, A., Alcántara, A., Lyamani, H., Alados-Arboledas, L.: Preliminary results of a non-spherical aerosol method for the retrieval of the atmospheric aerosol optical properties. *J. Quant. Spectrosc. Radiat. Transf.* **100**(1), 305–314 (2006)
14. Kobayashi, E., Uchiyama, A., Yamazaki, A., Kudo, R.: Retrieval of aerosol optical properties based on the spheroid model. *J. Meteorol. Soc. Jpn.* **88**(5), 847–856 (2010)
15. Dubovik, O., King, M.D.: A flexible inversion algorithm for retrieval of aerosol optical properties from sun and sky radiance measurements. *J. Geophys. Res.* **105**(D16), 20673–20696 (2000)
16. Van de Hulst, H.C.: *Light Scattering by Small Particles*. Dover, New York (1981)
17. Ghislan, R.F.: A new method for aerosol size distribution retrieval based on the anomalous diffraction approximation. In: *Proc. SPIE*, **4168**, pp. 243–248: (2000)
18. Sun, W.B., Fu, Q.: Anomalous diffraction theory for randomly oriented nonspherical particle: a comparison between original and simplified solutions. *J. Quant. Spectrosc. Radiat. Transf.* **70**(4–6), 737–747 (2001)
19. Xu, M., Lax, M.: Anomalous diffraction of light with geometrical path statistics of rays and a Gaussian ray approximation. *Opt. Lett.* **28**(3), 179–181 (2003)
20. Tang, H., Sun, X., Yuan, G.: Application on circular cylinder particle size distribution based on anomalous diffraction approximation. *Chin. J. Lasers* **34**(3), 411–416 (2007)
21. Tang, H.: Study of inversion algorithm of particle size distribution using total light scattering method. PhD thesis, Harbin: Harbin Institute of Technology. 2008.10
22. Paramonov, L.E.: Optical equivalence of isotropic ensembles of ellipsoidal particles in the Rayleigh-Gans-Debye and anomalous diffraction approximations and its consequences. *Opt. Spectrosc.* **112**(5), 787–795 (2012)
23. Gong, C., Wei, H., Li, X., Shao, S., Xu, Q., Chen, X.: The influence of the aspect ratio to the light scattering properties of cylinder ice particles. *Acta Opt. Sin.* **29**(5), 1155–1159 (2009)
24. Yamamoto, G., Tanaka, M.: Increasing of global albedo due to air pollution. *J. Atmos. Sci.* **29**(8), 1405–1412 (1972)
25. Whitby, K.T., Husar, R.B., Liu, B.Y.H.: The aerosol distribution of Los Angeles Smog. *J. Celluloid Interface Sci.* **39**(1), 177–204 (1973)
26. Zhao, J., Hu, Y.: Bridging technique for calculating the extinction efficiency of arbitrary shaped particles. *Appl. Opt.* **42**(24), 4937–4945 (2003)
27. King, M.D., Byrne, D.M., Herman, B.M., Reagan, J.A.: Aerosol size distribution obtained by inversion of spectral optical depth measurement. *J. Atmos. Sci.* **35**(11), 2153–2167 (1978)
28. Twomey, S.: *Introduction to the Mathematics of Inversion in Remote Sensing and Indirect Measurements*. Dover publication Inc., New York (1977)
29. Qiu, J., Wang, H., Zhou, X., Lv, D.: Experimental study of remote sensing atmospheric aerosol size distribution by combined solar extinction and forward scattering method. *Adv. Atmos. Sci.* **7**(1), 33–41 (1983)
30. Li, F., Liu, J., Lv, D.: Analyses of composite observation of optical properties of atmospheric aerosols in the late summer over some areas of North China. *Sci. Atmospherica Sin.* **19**(2), 235–242 (1995)
31. Mao, J., Sheng, H., Zhao, H., Zhou, C.: Observation study on the size distribution of sand dust aerosol particles over Yinchuan, China. *Adv. Meteorol.* **2014**, 1–7 (2014)
32. Vitale, V., Tomasi, C., Lupi, A., Cacciari, A., Marani, S.: Retrieval of columnar aerosol size distributions and radiative forcing evaluations from sun photo metric measurements taken during the CLEARCOLUMN (ACE2) experiment. *Atmos. Environ.* **34**(29–30), 5095–5105 (2000)
33. Heintzenberg, J., Muller, H., Quenzel, H., Thomalla, E.: Information content of optical data with respect to aerosol properties: numerical studies with a randomized minimization search technique inversion algorithm. *Appl. Opt.* **20**(8), 1308–1315 (1981)
34. Herman, B.M., Browning, S.R., Reagan, J.A.: Determination of aerosol size distributions from lidar measurements. *J. Atmos. Sci.* **28**(5), 763–771 (1971)
35. Ren, Y., Li, X., Lu, M., Hu, X.: Application prospect measurement by sun photometer CE318 and retrieval methodology. *Meteorol. Sci. Technol.* **34**(3), 349–352 (2006)

Publisher's Note Springer Nature remains neutral with regard to jurisdictional claims in published maps and institutional affiliations.